THRESHOLD GRAPHS ARE GLOBALLY SYNCHRONIZING

HONGJIN WU AND ULRIK BRANDES

ABSTRACT. Place n nodes on the unit circle and connect some pairs with springs that pull connected nodes toward each other. Which graphs always drive all nodes to converge to a single point, no matter where they start? This is known as the global synchronization problem of the Kuramoto model and is closely tied to the benign nonconvexity of its synchronization landscape. In this work, we show how this dynamical and continuous question can be reduced to a static and combinatorial one. We prove that threshold graphs, the graph class closed under adding isolated nodes and adding universal nodes, are globally synchronizing, based purely on a combinatorial analysis of unit-vector configurations in the plane. It is particularly striking that threshold graphs range from extremely sparse structures such as stars to the complete graph, suggesting that global synchronization in this class cannot be attributed to density. Our proof shows that global synchronization can instead emerge from a form of geometric symmetry.

Contents

1. Introduction	2
1.1. Notation	5
2. Preliminaries of threshold graphs	5
3. Preliminaries on Kuramoto synchronization	6
3.1. Equilibrium and local stability	7
3.2. Stationary point and local optimality	7
3.3. Correspondence between stability and geometry	7
3.4. Synchronous and aligned states	8
4. Combinatorial planar geometry of equilibrium	9
4.1. Vector-labelled graph	10
4.2. Alignment and equilibrium	10
4.3. Force and stability	12
4.4. Notations	15
5. Geometric twins and their phasor geometry	16
5.1. Closed geometric twins	16
5.2. Open geometric twins	17
6. Formation of geometric twins	18
6.1. Structural twins at equilibrium	19
6.2. Synchronous pendant extension	21
7. Main proof: the induction argument	24
7.1. One more key lemma	24
7.2. Illustrative example	25
7.3. Main proof	26
Acknowledgements	27
References	

Date: November 18, 2025.

1. Introduction

The study of synchronization traces back to the 17th century, when Christiaan Huygens first observed the spontaneous synchronization of pendulum clocks. Since then, synchronization phenomena have been widely studied across both natural and technological systems, from the flashing of fireflies [BB68, SS93] and the rhythmic beating of heart cells [Win67, MS06] to synchronization in power grids [DB13], and the Transformer architecture [GLPR23a, CRMB24]. The Kuramoto model, introduced by Yoshiki Kuramoto in 1975 [Kur75], strikes a balance between mathematical tractability and sufficient complexity, has become one of the key mathematical models for understanding the collective dynamics of coupled oscillators.

The Kuramoto model describes a system of n oscillators continuously evolving on the unit circle. Each vertex $i \in V$ corresponds to an oscillator with phase (angle) $\theta_i : \mathbb{R} \to \mathbb{S}^1$. The dynamics of phase θ_i of each oscillator evolves according to:

$$\frac{d\theta_i}{dt} = \omega_i + \sum_{j=1}^n \mathbf{A}_{ij} \sin(\theta_j - \theta_i), \tag{1}$$

This means that each oscillator's phase dynamics is governed by its intrinsic frequency ω_i while also being influenced by the phase differences with its neighbors in a nonlinear manner. There are two lines of research regarding this model focusing *heterogenous* and *homogenouse* case respectively.

Studies on the former case primarily consider a systems of oscillators with heterogenous intrinsic frequences $\{\omega_i\}_{i=1}^K$ coupled through a complete graph with identical weight $A_{ij} = \frac{K}{N}$. Here, K determines how strongly oscillators influence each other. A fundamental question in the heterogeneous setting is to determine the critical coupling strength K_c such that, for $K > K_c$, the oscillators achieve frequency synchronization, i.e., $\dot{\theta}_i - \dot{\theta}_j \to 0$, meaning that all oscillators rotate with the same angular velocity. If this indeed holds, it is natural to further ask whether the oscillators not only rotate with the same angular velocity, but also converge to the same phase, known as phase synchronization, that is, whether $\theta_i - \theta_j \to 0$, as $t \to \infty$. The study of synchronization in the heterogeneous Kuramoto model is particularly relevant to real-world systems. In many natural and engineered networks such as power grids, neuronal circuits, and circadian rhythms, the individual oscillators typically have distinct natural frequencies. Within this heterogeneous setting, a rich variety of nonlinear dynamical phenomena can emerge, including partial synchronization, multistability, and even chaotic behavior. For further background and details, we refer the reader to [Str00, ABV⁺05, DB14].

Recent works on the Kuramoto model has moved beyond the fully connected case to more general interaction graphs. Such settings are not only mathematically appealing but also more realistic, since interactions in natural and engineered systems are rarely all-to-all. In this work, we focus on the homogeneous case with identical intrinsic frequencies ($\omega_i = \omega$ for all i) and aim to understand how graph structure governs synchronization. To begin with, we first remark that in this case, frequency synchronization always holds and the remaining question is whether phase synchronization can be achieved. This is not obvious if we only look at the equation $\dot{\theta}_i = \omega + \sum_{j=1}^{n} A_{ij} \sin(\theta_j - \theta_i)$, for all i, since it tells that the instantaneous angular velocity of each node depends both on this common intrinsic term and on the coupling with its neighbors. However, applying a co-rotating frame $\theta_i(t) \leftarrow \theta_i(t) - \omega t$, the equations becomes

$$\frac{d\theta_i}{dt} = \sum_{j=1}^n \mathbf{A}_{ij} \sin(\theta_j - \theta_i), \quad i \in \{1, \dots, n\},$$
(2)

and this reduced system is in fact a gradient flow of the Kuramoto energy function

$$E(\theta) = \frac{1}{2} \sum_{1 \le i \le j \le n} \mathbf{A}_{ij} (1 - \cos(\theta_i - \theta_j))$$
(3)

as its gradient satisfies $\dot{\theta}_i dt = -\frac{\partial E}{\partial \theta_i}$. By LaSalle's invariance principle, every trajectory converges to the invariant set of equilibria satisfying $\dot{\theta}_i = 0$ for all i. Hence, the angle differences do not lead to frequency discrepancies in the asymptotic sense. In other words, frequency synchronization always holds, as they share common frequency ω . Now the real challenge in the homogeneous case lies in understanding whether phase synchronization can always be achieved, regardless of the initial phase configurations. It is evident that this property is entirely determined by the graph structure, since the adjacency matrix $\bf A$ of the graph is the only external parameter in the homogeneous Kuramoto model (2) and equivalently in its energy formulation (3). Thus, we define:

Definition 1.1 (Globally synchronizing graph). We say that a graph G with adjacency matrix A is *globally synchronizing* if, all oscillators converge to the same phase, i.e.,

$$\lim_{t \to \infty} \theta_i(t) - \theta_j(t) = 0 \quad \text{for all } i, j \in V.$$

for all initial conditions $\theta(0) \in \mathbb{R}^n$ except for a set of measure zero. In other words, almost all trajectory converges to the synchronous state $\theta_i = \theta_j$, for all $i, j \in V(G)$.

The key question is now stated as:

On which graphs, the Kuramoto model (2) exhibits global synchronization?

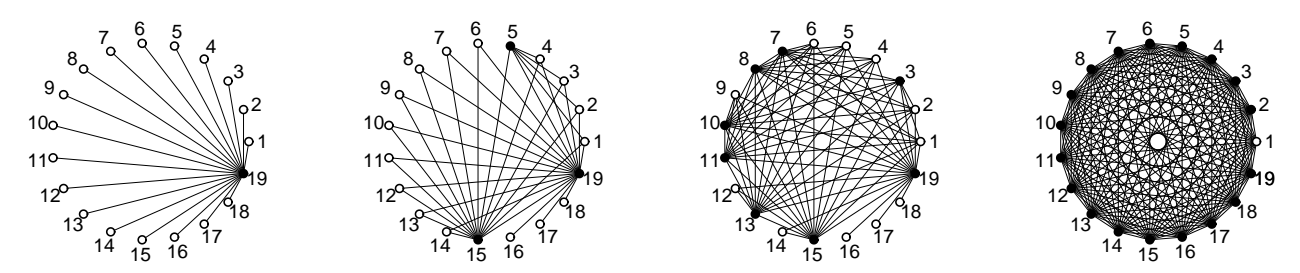
This seemingly simple description conceals a mathematically challenging task. To address this problem, we note that the Kuramoto model (2) can be formulated as a gradient flow of the energy function (3), as mentioned before. Hence, understanding the geometry of (3) provides direct insight into the long-term dynamics of (2). In particular, the synchronous states correspond exactly to the global minima of this energy function, and those minima that are local but not global (called *spurious local minimua*) correspond to non-synchronous equilibria. If such spurious local minima exist, the gradient dynamics may converge to them whenever the initialization lies within their basin of attraction, in which case the graph G is not globally synchronizing. In contrast, if the energy function admits no spurious local minima, then the graph G is globally synchronizing, since this rules out convergence to any non-synchronous equilibrium except possibly for a set of initial conditions of measure zero. A rigorous proof of this statement can be established using the Lojasiewicz gradient inequality together with the center manifold theorem; see Lemma A.1 in [GLPR23b] for an excellent exposition.

Contributions and prior work. Aiming to understand which graphs and how them foster global synchronization, previous studies on this problem can be broadly divided into two lines of research: (i) investigating whether random graphs globally synchronize, and (ii) determining the minimum edge density required to ensure global synchronization. Both approaches are, in a certain sense, grounded in the fact that the complete graph is globally synchronizing, and that both random graphs and very dense graphs tend to behave like complete graphs. Intuitively, a graph of sufficiently high density becomes homogeneous enough to approximate a complete graph. In this sense, full connectivity is not strictly required, that is, global synchronization can still emerge with a small gap from the fully connected case.

In this work, we prove that *threshold graphs*, as a graph class that by no means closed to complete, but still globally synchronize.

(i) What are threshold graphs? Threshold graphs can be constructed starting from a single vertex by iteratively adding each new vertex as either: an isolated vertex connecting to no existing vertex, or

a dominating vertex connecting to all existing vertices. This generative process is uniquely encoded by a binary sequence of length n-1, where 0 denotes an isolated vertex and 1 a dominating one. Thus our goal is to show all threshold graphs with sequence ending by 1 must globally synchronizes, because otherwise it is not connected.



(ii) Why threshold graphs? Many theorems start from initial observations, from which suitable conjectures are formulated. Our case is no exception. Our investigation into global synchronization on threshold graphs began with a simple observation: complete graphs and star graphs, respectively the densest and sparsest connected graphs in the class of threshold graphs, both exhibit global synchronization. Certainly, this is not sufficient to propose the conjecture that all threshold graphs globally synchronize. Indeed, although the two extremes synchronize, this does not necessarily imply that the entire spectrum of threshold graphs does.

However, two further observations strengthened our confidence in this conjecture. Firstly, in threshold graphs, the neighborhoods of any two nodes are nested: for any pair u, v, either $N[u] \subseteq N(v)$ or $N[v] \subseteq N(u)$. This total preorder of vicinities suggests that influence may propagate step by step from the most dominant node to the rest without interference, hinting at the possibility of global synchronization. Secondly, no counter-example was found in our numerical experiments up to 50 size graphs¹. These evidence encourages us to investigate whether all connected threshold graphs global synchronize. In particular, we established the following result:

Theorem 1.2. Any connected threshold graph globally synchronizes.

Many existing proofs of global synchronization rely, either explicitly or implicitly, on the so-called half-circle lemma. This lemma states that if all oscillators are confined to an open half-circle, then their dynamics will contract toward synchrony. Based on this observation, the bootstrap strategy attempts to show that all second-order critical points must lie within a half-circle. If successful, this rules out the existence of non-synchronous equilibria and thereby implies global synchronization.

However, for threshold graphs, it remains unclear how to apply this strategy. It typically depends on sufficient connectivity in the network thus naturally suited to dense graphs, where the large number of edges ensures that nodes inside the half-circle collectively exert sufficient force to pull outside nodes back into alignment. In contrast, threshold graphs span the full spectrum from

¹First, we transform the equilibrium equations of the Kuramoto model into a system of polynomial equations. We then use Bertini software package [BHSW13] to compute the zeros of this system, and subsequently evaluate the Jacobian at each solution to determine their stability.

extremely sparse examples such as stars to dense cliques, and their highly inhomogeneous, layered structure complicates the application of this strategy. As a result, existing techniques offer limited insight into whether and why these graphs synchronize globally.

In this work, we bypass the half-circle approach by reducing the high-dimensional geometric question of whether the energy landscape is benign to a planar vector-geometry condition. This condition naturally leads us to study *structural twins* (pairs of nodes sharing the same neighborhood in the graph) as well as a new notion we introduce, that of *geometric twins* (a broader concept depending jointly on the graph structure and the equilibrium configuration θ). These notions clarify how the relative positions of phasors behave at second order stationary point of the energy landscape $\mathbb{E}(\theta)$. Building on this understanding, we employ an inductive strategy: synchronization is first established locally on small substructures, and then shown to propagate across the whole graph along the neighborhood-inclusion hierarchy of threshold graphs.

(iii) What we learned from global synchrony of threshold graphs? While identifying previously unknown classes of globally synchronizing graphs contributes to the expansion of known results, a more fundamental objective of this line of research is to elucidate the mechanisms that give rise to global synchronization itself. It is already known that for certain classes of graphs, global synchronization arises through mechanisms that, in a certain sense, are close to those of complete graphs. Threshold graphs, however, lie outside this regime. Nevertheless, we prove in this work that they also exhibit global synchronization. What deeper insight can we draw from this result?

Our analysis shows that the synchronization of threshold graphs is instead driven by another mechanism, namely their intrinsic symmetries. These symmetries are not merely combinatorial, such as sets of nodes sharing identical neighborhoods, but are geometric in nature. We will introduce this notion in detail later, but to give an intuition, these geometric symmetries emerge inductively as the graph is reduced node by node. Through this process, we uncover certain sets of nodes that, while not symmetric in the structural sense of graph theory, exhibit geometric symmetry at the second-order critical points of (3), which allows us to show that these nodes form a synchronized group. As the reduction continues, more geometric symmetries are revealed, leading to the formation of progressively larger synchronized groups, until the entire node set forms a single synchronized group, thereby guaranteeing that all second order critical points are synchronized states, thus the graph is global synchronizating.

1.1. **Notation.** Throughout this work, we consider only connected simple graphs, i.e., graphs without self-loops or weighted edges. Furthermore, since the homogeneous Kuramoto model (2) on G is fully determined by the graph topology, we sometimes use system G to denote the Kuramoto model on this graph for simplicity. Following the convention of dynamical systems, we refer to the variable $\theta = (\theta_1, \dots, \theta_n)$ of the Kuramoto model (2) as a state, and call the solution $\theta(t)$ with respect to the initial condition $\theta(0)$ in the Kuramoto model (2) a trajectory starting from $\theta(0)$.

2. Preliminaries of threshold graphs

Threshold graphs are a well-studied class of graphs that play a central role in graph theory and have found applications across various disciplines. They were in fact discovered independently and reported in different journals by researchers working in distinct fields. The term "threshold graph" was introduced by Chvátal and Hammer in their study of set-packing problems. Around the same time, the same class of graphs was independently discovered by Henderson and Zalcstein in the context of parallel processing, where they were referred to as PV-chunk definable graphs. Since then, threshold graphs have appeared in various contexts, including resource allocation, cyclic

scheduling, manpower planning, complexity theory, and the study of graphical degree sequences.

Many equivalent conditions have been found for threshold graphs including constructive forms and forbidden configurations. See for example [MP95] for nine different characterizations.

Definition 2.1. A graph is threshold if it contains no induced P_4 , C_4 and $2K_2$.

One of the many characterizations of threshold graphs is constructive. The construction is in terms of two basic operations; adding a disjoint vertex (adjacent to no existing vertex), or a dominating vertex (adjacent to all existing vertices).

The construction process can be encoded into a binary sequence, called *threshold sequence*, that is $(b_1, \ldots, b_n) \in \{0, 1\}^n$ such that starting from a single vertex, for each $b_i = 0$ we add an isolated vertex, and for each $b_i = 1$ we add a dominating vertex; see Figure 1.

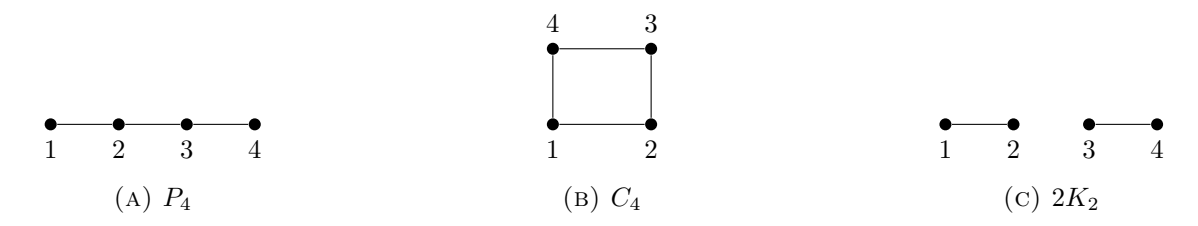


FIGURE 2. Forbidden induced subgraphs for threshold graphs: graphs are $\{P_4, C_4, 2K_2\}$ -free. Only edges within each induced pattern are drawn.

Remark 2.2. Interestingly, threshold graphs have also been studied in synchronization contexts beyond oscillator models. In particular, [PS95] surveyed their use in the design of synchronization protocols for cooperating processes, focusing on mutual exclusion via semaphore-based control mechanisms and the so-called PV-chunk semaphores. In some papers, these are also referred to as Pv_c -definable graphs.

3. Preliminaries on Kuramoto Synchronization

In this section, we aim to establish the correspondence between dynamical and optimization concepts in the homogeneous Kuramoto model. Since the homogeneous Kuramoto model (2) can be formulated as a gradient dynamical system with the energy function (3) and the real analycity of (3), the dynamical notions of equilibrium points and stable equilibria naturally correspond to the optimization notions of first-order and second-order stationary points of the energy function. Before showing this correspondence, we first provide the formal definitions of (stable) equilibria in dynamical systems and of first- and second-order stationary points in optimization. It is worth noting that such a one-to-one correspondence between the two sets of concepts is rather uncommon. This special structure is precisely what allows the analysis of global synchronization in the Kuramoto model to be directly connected to the geometry of the nonconvex optimization landscape.

In general, the evolution of a dynamical system can often be viewed as a descent process of a potential, known as a Lyapunov function, which monotonically decreases along the system trajectories. However, Lyapunov functions are not unique in general, let alone the existence of a clear correspondence between the two classes of concepts discussed above. Moreover, even if the system is of gradient type so that its energy function serves as a natural candidate for a Lyapunov function, such a correspondence is still not guaranteed in general. The remarkable property of the homogeneous Kuramoto model considered here is that its energy function is real analytic, and it is precisely this property that ensures the correspondence between dynamical and optimization notions. For further discussion and proofs, we refer the reader to [AK06].

3.1. Equilibrium and local stability. In this section, we introduce the notion of *equilibrium* and stable equilibrium of the Kuramoto model (2).

By the definition, equilibrium points of a dynamical system are the points where the system remains at rest, meaning that the first-order derivative of the state vanishes [Kha02]. Setting the right-hand side of (2) to zero provides the characterization of an equilibrium point in the homogeneous Kuramoto model on the graph G.

Definition 3.1 (Equilibrium of the Kuramoto model (2)). We call $\theta \in \mathbb{R}^n$ an equilibrium of the Kuramoto model (2) if it satisfies

$$\sum_{j=1}^{n} \mathbf{A}_{ij} \sin(\boldsymbol{\theta}_j - \boldsymbol{\theta}_i) = 0, \quad \forall i \in [n].$$
(4)

An equilibrium point is considered stable if small perturbations around it remain small over time [Kha02]. The linearization of a nonlinear system provides a necessary condition for local stability: an equilibrium point is stable if the *Jacobian* matrix is negative semi-definite.

Proposition 3.2 (Characterization of stable equilibrium). An equilibrium point θ is stable if the Jacobian matrix J, defined as:

$$\mathbf{J}_{ij} = \begin{cases} -\sum_{j=1}^{n} \mathbf{A}_{ij} \cos(\theta_i - \theta_j), & \text{if } i = j, \\ \mathbf{A}_{ij} \cos(\theta_i - \theta_j), & \text{if } i \neq j, \end{cases}$$

is negative semi-definite.

3.2. Stationary point and local optimality.

Definition 3.3 (Stationary point of the energy function (3)). We call $\theta \in \mathbb{R}^n$ a stationary point of the energy function (3) if it satisfies $\nabla E(\theta) = 0$, namely

$$\sum_{i=1}^{n} \mathbf{A}_{ij} \sin(\boldsymbol{\theta}_j - \boldsymbol{\theta}_i) = 0, \quad \forall i \in [n].$$
 (5)

Obviously, from Proposition 3.1 and Definition 3.3, a configuration $\theta \in \mathbb{R}^n$ is a stationary point of the energy function (3) if and only if it is an equilibrium of the Kuramoto model (2).

Definition 3.4 (Local minimum of the energy function). A configuration $\theta \in \mathbb{R}^n$ is called a *local minimum* of the energy function E if there exists $\varepsilon > 0$ such that

$$E(\theta) \le E(\theta'), \quad \forall \theta' \in \mathbb{R}^n \text{ with } \|\theta' - \theta\| < \varepsilon.$$

Proposition 3.5 (First- and second-order necessary conditions). If a configuration θ is a local minimum of E, then

- (1) $\nabla E(\theta) = 0$ (first-order condition), and
- (2) the Hessian $\nabla^2 E(\theta)$ is positive semidefinite.

A point satisfying the above two conditions is also called a second-order stationary point (SOSP) of (3).

3.3. Correspondence between stability and geometry. In this section, we briefly outline the relationship between equilibrium stability in the dynamical system (2) and the geometric structure of the energy function (3). Understanding this correspondence provides valuable intuition. In particular, in this work, we often exploits the fact that a small perturbation causes the system to leave that state (therefore this state in unstable), in order to show a certain state is not a second-order critical point.

At the first-order level, the two notions coincide: a configuration θ is a critical point of the energy function $E(\theta)$ if and only if it is an equilibrium of the dynamical system (2), since both are characterized by

$$\sum_{i=1}^{n} A_{ij} \sin(\theta_i - \theta_j) = 0 \text{ for all } i \in [n]$$

One can further relate the stability of an equilibrium to second-order conditions of the energy landscape. It is precisely because of the real analycity of the energy function (3), the local asymptotic stability of an equilibrium of (2) is equivalent to the local minimality of the energy function (3). This is a remarkable property since it does not hold in general for dynamical systems. In general, the dynamics of a system may admit more complex behaviors near equilibria such as limit cycles, or chaotic dynamics, etc. The relation mentioned here is summarized in Figure 3. One can find the proof in the celebrated work [AK06].

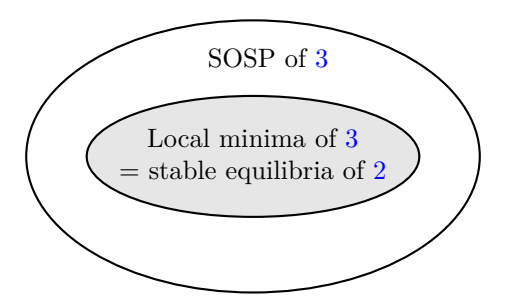


FIGURE 3. Relation between different concepts. Here equivalence between stable equilibrium and local minimum is established in [AK06].

3.4. Synchronous and aligned states. In this section, we prove that all aligned states are equilibria. Among them, however, the non-synchronous ones are not second-order stationary points (SOSPs). Before that, we first define the notions of synchronous states and aligned states.

Definition 3.6. A state $(\theta_1, \dots, \theta_n)$ of G = (V, E) is called a *synchronous state* if for all $i, j \in V$, $\theta_i \equiv \theta_i \pmod{2\pi}$.

More generally, it is called an *aligned state* if for all $i, j \in V$,

$$\theta_i \equiv \theta_j \pmod{\pi}$$
.

Clearly, every synchronous state is also an aligned state. The stability of all aligned states is:

Theorem 3.7. Any aligned state is an equilibrium of the Kuramoto model (2) on the graph G or equivalently stationary point of $E(\theta)$. Among them, synchronous states are second-order critical point of (3)², while non-synchronous aligned states are not second-order critical point of (3).

Proof. Firstly, it is straightforward to see that aligned states satisfy the condition (4), therefore they are equilibria of G, or equivalently stationary point of $E(\theta)$.

Secondly, we turn to the second-order criticality of synchronous states. The Hessian matrix at synchronous states is given by

$$\mathbf{H}_{ij} = \begin{cases} \sum_{j=1}^{n} \mathbf{A}_{ij}, & \text{if } i = j, \\ -\mathbf{A}_{ij}, & \text{if } i \neq j, \end{cases}$$
 (6)

²In fact, they are asymptotically stable equilibria up to rotational invariance

Clearly, **H** is the Laplacian matrix \mathcal{L} of the graph G. Note that \mathcal{L} is a positive semidefinite matrix with only one zero eigenvalue, due the connectness of graph G. Therefore, **H** is a positive semidefiniteness matrix, implying that any synchronous state is second-order stationary point of $E(\theta)$.

Thirdly, regarding the second-order criticality of non-synchronous aligned states. Without loss of generality³, assume $\theta_i = 0$ or π , for any $i \in [n]$. Let $\mathbf{x} = (x_1, \dots, x_n)$ be an n-dimensional vector that indicates which group (either at angle 0 or π) each node belongs to

$$x_i = \begin{cases} 1, & \text{if } \theta_i = 0\\ -1, & \text{if } \theta_i = \pi \end{cases}$$
 (7)

Then the Hessian matrix at any antipodal state is not negative semidefiniteness. Indeed, this can be inferred by the quadratic form

$$\boldsymbol{x}^T \mathbf{H} \boldsymbol{x} = \sum_{i \mid \theta_i = 0} \sum_{j \mid \theta_j = \pi} \boldsymbol{A}_{ij} \cos(\theta_i - \theta_j) = -\sum_{i \mid \theta_i = 0} \sum_{j \mid \theta_j = \pi} \boldsymbol{A}_{ij} < 0$$

since $A_{ij} \geq 0$, and there must exist at least one pair of nodes i, j such that $\theta_x \equiv \theta_y \pmod{\pi}, k \in \mathbb{Z}$, given the connectness of G. Therefore, any non-synchronous aligned state is not a SOSP.

Remark 3.8. In fact, synchronous states are asymptotically stable equilibria up to a global rotation. Here, asymptotic stability is a stronger notion than mere stability: it requires that small perturbations lead to trajectories returning to the equilibrium. On the other hand, non-synchronous aligned states are not SOSPs and therefore cannot be local minima of 3 or say not stable equilibrium of 2.

The instability of non-synchronous states can be intuitively understood as follows: a set of antipodally positioned oscillators must evolve in a way that decreases the system's energy, as there always exists an interaction force between these antipodal pairs that drives them closer together.

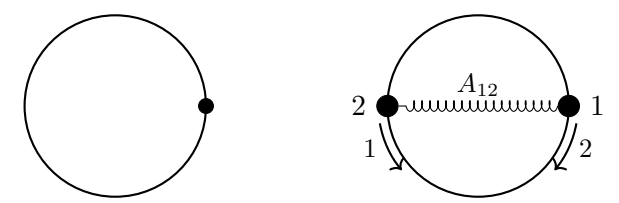


FIGURE 4. Synchronous (left) and non-synchronous aligned state (right). Arrows indicate the nodes moving closer along the circle, implying this state is not stable.

4. Combinatorial planar geometry of equilibrium

As we will introduce later, the key idea of our proof is to assume that a configuration θ is a second-order critical point and show that this assumption forces θ to be synchronized, meaning that all node vectors coincide. This requires us to understand the geometric configuration of second-order critical points on the unit circle. In the previous section, we presented the algebraic conditions characterizing first- and second-order critical points.

In this section, we employ a complex-number formulation to transform these algebraic conditions into geometric ones, i.e., combinatorial relations between the vectors associated with the nodes. This seemingly simple transformation significantly simplifies the original landscape geometry problem, reducing it to a combinatorial-geometric problem involving vectors on the two-dimensional plane. With this, one just needs to understand whether, under the geometric form of the first- and second-order conditions, it can be deduced that all vectors must be identical.

³Any aligned state can be rotated uniformly on all angles $\theta_1, \dots, \theta_n$, such that $\theta_i = 0$ or π , for any $i \in [n]$.

4.1. Vector-labelled graph. Given a state $\theta \in \mathbb{R}^n$, we associate to each node $i \in V$ its phasor $\mathbf{v}_i := (\cos \theta_i, \sin \theta_i) \in \mathbb{R}^2$.

This yields a vector-labeled graph $(G, \{v_i\}_{i \in V})$ which encodes the phase configuration $\boldsymbol{\theta}$ geometrically.

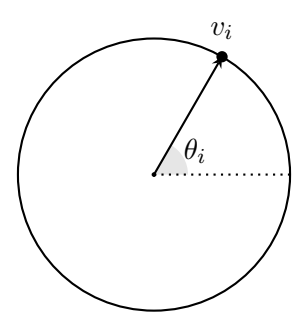


FIGURE 5. Representation of v_i with angle θ_i .

Although straightforward to construct, this object captures both the equilibrium condition and its stability in the Kuramoto model (2) on the graph G.

More precisely, to determine whether a given θ is an equilibrium and whether it is stable (or more general, second-order critical point), the combinatorial geometry of the vector-labeled graph $(G, \{v_i\}_{i\in V})$ provides a geometric view to algebraic one (solving nonlinear equations and analyzing Hessian at stationary point), as detailed in Section 4.2.

4.2. Alignment and equilibrium. Given a vector-labeled graph $(G, \{v_i\})$, we now formulate the equilibrium condition of (2) in geometric terms. For each node $i \in V$, we aggregate the phasors of its neighbors into a single vector:

$$\sum_{j\in N(i)} \boldsymbol{v}_j.$$

This vector represents the aggregated state of node i's neighbors. If it is not aligned with v_i , then intuitively, due to the intrinsic synchronization mechanism in the Kuramoto model, the nodes will tend to move toward alignment instead of staying there at rest, therefore not in equilibrium. The equivalence between the alignment $\sum_{j \in N(i)} v_j \parallel v_i$ for every node $i \in V$ and the equilibrium condition can be rigorously established by representing the phasors as complex numbers.

Lemma 4.1 (Equilibrium condition rephrased geometrically). A state θ is an equilibrium of the Kuramoto model (2) on G = (V, E) with adjacency A if and only if, for each $i \in V$,

$$\sum_{j \in N(i)} \mathbf{v}_j = \mu_i \mathbf{v}_i \quad \text{where} \quad \mu_i = \sum_{j \in N(i)} \cos(\theta_j - \theta_i). \tag{8}$$

Proof of Lemma 4.1. Let us firstly derive an equivalent form of (8). Rewrite all vectors \mathbf{v}_i in (8) in terms of their Cartesian components $(\cos \theta_i, \sin \theta_i)$, yielding

$$\sum_{j \in N(i)} (\cos \theta_j, \sin \theta_j) = \mu_i(\cos \theta_i, \sin \theta_i).$$

Equivalently, this can be written as

$$\begin{cases}
\sum_{j \in N(i)} \cos \theta_j = \mu_i \cos \theta_i, \\
\sum_{j \in N(i)} \sin \theta_j = \mu_i \sin \theta_i.
\end{cases}$$
(9)

This is equivalent to verifying the equality between two complex numbers:

$$\sum_{j \in N(i)} \cos \theta_j + I \sum_{j \in N(i)} \sin \theta_j = \mu_i \cos \theta_i + I \mu_i \sin \theta_i,$$

which can be compactly rewritten as

$$\sum_{j \in N(i)} e^{I\theta_j} = \mu_i e^{I\theta_i}. \tag{10}$$

using the Euler formula $e^{I\theta_i} = \cos \theta_i + I \sin \theta_i$. Now that we have derived the equivalence between conditions (8) and (10), our goal now reduces to proving the equivalence between (10) and (3), namely

$$\sum_{j \in N(i)} e^{I\theta_j} = \mu_i e^{I\theta_i} \Longleftrightarrow \sum_{j \in N(i)} \sin(\theta_j - \theta_i) = 0.$$

This indeed holds.

To prove the implication from the right-hand side to the left-hand side, we construct such a μ_i that satisfies the left-hand side. Dividing both sides of (10) by $e^{I\theta_i}$ (noting that $e^{I\theta_i} \neq 0$), we obtain

$$\frac{\sum_{j \in N(i)} e^{I\theta_j}}{e^{I\theta_i}} = \mu_i.$$

Such a μ_i exists and is in fact given by

$$\mu_i = \sum_{j \in N(i)} \cos(\theta_j - \theta_i),$$

at an equilibrium point θ , as we will show below. Expanding the fraction, we obtain

$$\frac{\sum_{j \in N(i)} e^{I\theta_j}}{e^{I\theta_i}} = \sum_{j \in N(i)} e^{I(\theta_j - \theta_i)}$$

$$= \sum_{j \in N(i)} (\cos(\theta_j - \theta_i) + I\sin(\theta_j - \theta_i)).$$
(11)

Since θ is an equilibrium, the imaginary part must vanish, leading to

$$\frac{\sum_{j \in N(i)} e^{I\theta_j}}{e^{I\theta_i}} = \sum_{j \in N(i)} \cos(\theta_j - \theta_i) \in \mathbb{R}.$$

Thus, we conclude

$$\sum_{j \in N(i)} e^{I\theta_j} = \sum_{j \in N(i)} \cos(\theta_j - \theta_i) \cdot e^{I\theta_i}.$$

Conversely, to prove the left-hand side implies the right-hand side, we show that if there exists a constant μ_i such that

$$\sum_{j \in N(i)} e^{I\theta_j} = \mu_i e^{I\theta_i},$$

then θ is an equilibrium point. This is equivalent to showing that

$$I\sum_{j\in N(i)}\sin(\theta_j-\theta_i)+\sum_{j\in N(i)}\cos(\theta_j-\theta_i)\in\mathbb{R}.$$

Indeed, we compute

$$I \sum_{j \in N(i)} \sin(\theta_j - \theta_i) + \sum_{j \in N(i)} \cos(\theta_j - \theta_i)$$

$$= \sum_{j \in N(i)} e^{I(\theta_j - \theta_i)}$$

$$= \frac{\sum_{j \in N(i)} e^{I\theta_j}}{e^{I\theta_i}}$$

$$= \mu_i.$$
(12)

Thus, the proof is complete.

Remark 4.2 (Normalization and local coherence). One can rewrite (4.1) into

$$\mathbf{v}_i = \frac{1}{\mu_i} \sum_{j \in N(i)} \mathbf{v}_j, \quad where \ \mu_i = \left\| \sum_{j \in N(i)} \mathbf{v}_j \right\| = \sum_{j \in N(i)} \cos(\theta_j - \theta_i).$$

The expression describes a geometric condition of equilibrium: At equilibrium, each phasor aligns with the direction of the sum of its neighbors' vectors and is scaled to unit length. Although introduced as a normalization factor, the quantity μ_i carries physical meanings. If the neighbors are highly coherent, the sum vector is large, requiring a larger μ_i to normalize \mathbf{v}_i to unit length; if the directions are dispersed, μ_i is small. In this sense, μ_i measures how strongly the phasors of node i's neighbors align directionally. Indeed, defining the local order parameter

$$R_i := \frac{1}{\deg(i)} \left| \sum_{j \in N(i)} e^{i\theta_j} \right|,$$

we have the relation $\mu_i = \deg(i) \cdot R_i$, showing that μ_i is proportional to the standard notion of local phase coherence.

Remark 4.3 (Equilibrium and force). This equation admits a natural physical interpretation using the concept of force. Write each phasor \mathbf{v}_i in complex form as $e^{i\theta_i}$. Then, intuitively, each neighboring node $j \in N(i)$ pulls node i with a force given by $e^{I(\theta_j - \theta_i)}$. Under this interpretation, equation (4.1) states that: At equilibrium, the total force acting on node i sums to a real scalar. In other words, the net force is purely radial and contributes only to scaling. Due to the unit circle geometry $|\mathbf{v}_i| = 1$ of the Kuramoto model, such a scaling force does not induce any motion while a tangential component can cause rotation.

Notation. (1) We will call $\boldsymbol{\theta}$ is an equilibrium of G receives the force $\boldsymbol{\mu} = (\mu_1, \dots, \mu_n)$, if the vetor-labaled graph representation of $\boldsymbol{\theta}$ satisfies (4.1). Note that, in such case, $\mu_i = \sum_j A_{ij} \cos(\theta_j - \theta_i)$, for all $i \in V$; (2) At state $\boldsymbol{\theta}$, we say that node $i \in V$ is at equilibrium at $\boldsymbol{\theta}$ with respect to G if there exists a scalar μ_i such that (8) holds. Clearly, if $\boldsymbol{\theta}$ is an equilibrium, then every node $i \in V$ is at equilibrium. In particular, we call a node i is positively (or negatively, or zero) forced, if $\mu_i > 0$ (or < 0, or = 0).

4.3. Force and stability. Having established the correspondence between vector alignment at each node and the equilibrium condition, we now turn to the question of stability.

Alignment alone does not guarantee stability. Intuitively, if there exists a node i such that the angle between v_i and the resultant vector $\sum_{j \in N(i)} v_j$ is zero, a small perturbation will cause the system to return to equilibrium, much like a ball resting at the bottom of a potential valley. In contrast, if the angle is π , the system is analogous to a ball positioned at the peak of a hill: although it is momentarily at rest, a small perturbation will cause the ball to roll away.

In this section, this intuition is formally confirmed by using the relationship between the negative semi-definiteness of the Jacobian and its diagonal entries, as well as the connection between the stability of equilibrium in gradient dynamical systems and the local geometry of the corresponding energy function.

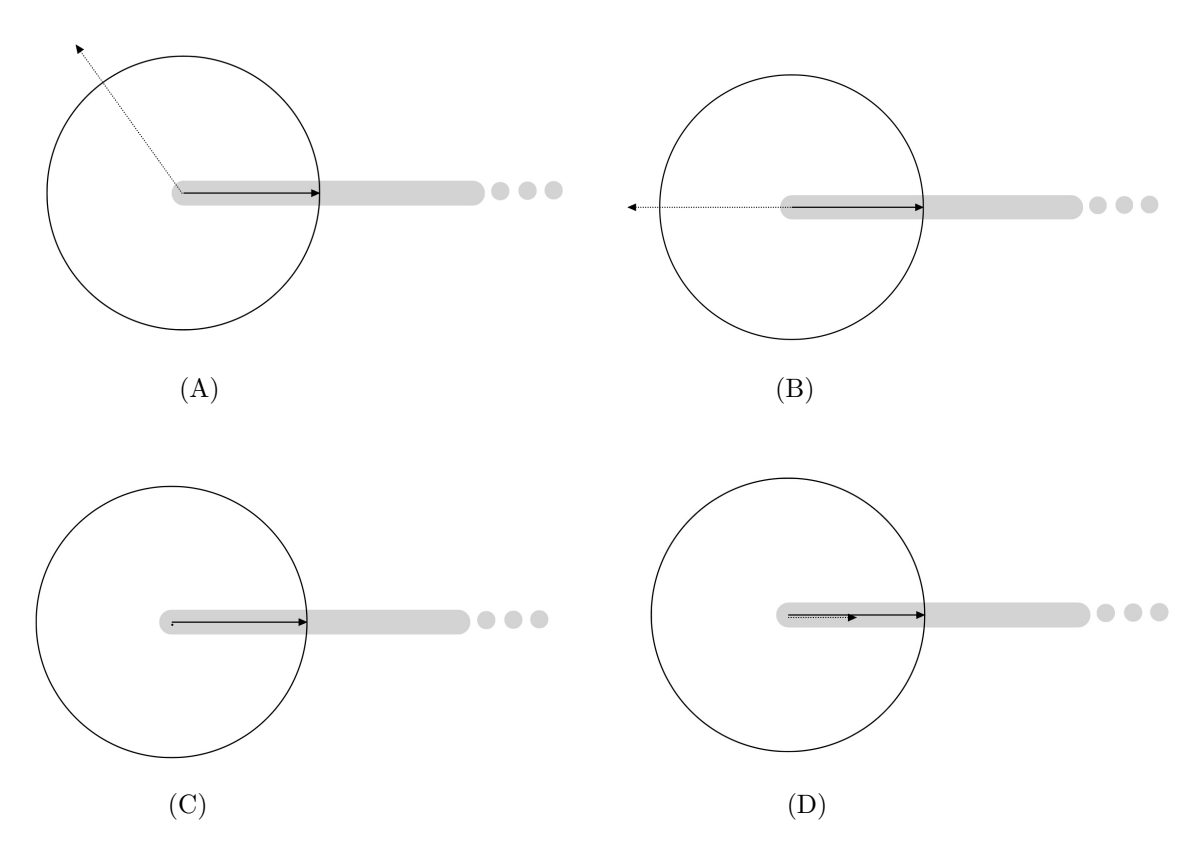


FIGURE 6. Illustration of different stability conditions for node i. Here, the solid arrow represents v_i , while the dashed arrow represents $\sum_{j \in N(i)} v_j$. The gray region indicates that, in order for node i to attain equilibrium under non-negative forcing, the endpoint of $\sum_{j \in N(i)} v_j$ must lie within this sector. (A) Node i is not at equilibrium since (8) does not hold; (B) Node i is at equilibrium but negatively forced, and thus unstable. Therefore, θ cannot be a second-order critical point. In cases (C) and (D), node i is at equilibrium, and is zero forced and positively forced respectively. Thus, satisfies the necessary condition for θ to be a second-order critical point.

Lemma 4.4. Assume θ is an equilibrium state of system G = (V, E) or equivalently first order stationary point of (3). In other words, there exist real numbers μ_1, \ldots, μ_n such that for all $i \in V$,

$$\sum_{j=1}^n A_{ij} \boldsymbol{v}_j = \mu_i \boldsymbol{v}_i.$$

If θ is a second order stationary point of (3), then all μ_i must be non-negative.

Remark 4.5 (Mechanical insight into node at stable equilibrium). The equilibrium condition in Lemma 4.4 for node $i \in V$ has a mechanical interpretation. The sum of the phasors representing its neighbors can be visualized as a set of unit-length rods with directions. We place one phasor's starting point at the origin, then connect the remaining phasors head-to-tail. The head-to-tail

connected rods can freely adjust their orientations, but the endpoint of the last phasor must remain on the right-end unrestricted sliding track, to ensure node i being stable there.

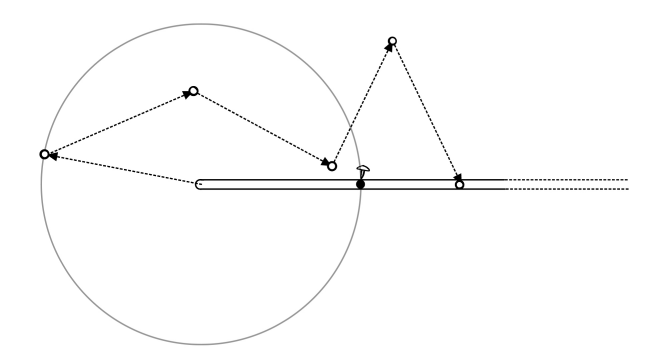


FIGURE 7. v_i is pinned down at zero angle, which determines the region where $\sum_{j=1}^{n} A_{ij}v_j$ should be (the right-end unrestricted region). The dashed vectors represent the phasors of nodes connected to i.

Proof of Lemma 4.4. We begin by noting that the *i*-th diagonal entry of the Hessian matrix **H** at $(\theta_1, \dots, \theta_n)$ can be rewritten as

$$\mathbf{H}_{ii} := \sum_{j=1}^{n} \mathbf{A}_{ij} \cos(\theta_i - \theta_j) = \sum_{j=1}^{n} \mathbf{A}_{ij} e^{I(\theta_j - \theta_i)} = \mu_i$$

where the second equality uses the equilibrium condition (4.1), and the last equality is deduced from re-writing the unit vectors in condition $\sum_{j=1}^{n} A_{ij} v_j = \mu_i v_i$ into the form using complex numbers. If there exists $\mu_i < 0$, then equivalently $\mathbf{H}_{ii} < 0$, which contradicts the positive definiteness of \mathbf{H} , see [Bha07] [HJ85]. Hence, $\boldsymbol{\theta}$ cannot be a second-order critical point. Consequently, it is neither a local minimum of (3) nor a stable equilibrium of (2). Therefore, $\mathbf{H}_{ii} = \mu_i > 0$ holds for all $i \in [n]$, where n is the size of G.

To summarize, the lemma above shows that at any second-order critical point θ , the phasor of each node must be positively aligned with the sum of the phasors of its neighbors (whenever the latter is nonzero). That is,

$$v_i \, \uparrow \sum_{j=1}^n A_{ij} v_j \quad \text{or} \quad \sum_{j=1}^n A_{ij} v_j = \mathbf{0},$$

for all $i \in [n]$.

Notation. Here, We write $a \uparrow b$, if both are nonzero and point in the same direction (i.e., the angle between them is zero). In the remainder of this manuscript, we will use this notation, as we find it more intuitive.

Remark 4.6 (This is only a necessary condition). Conversely, at a critical point (equilibrium), all $\mu_i > 0$ for all $i \in V$ is not sufficient to guarantee that $\boldsymbol{\theta}$ is a second-order critical point. As a counter-example, the equilibrium $\boldsymbol{\theta}^* = (0,0,0,0,\pi,\pi,\pi,\pi)$ of the Kuramoto model on the graph in Figure 8 is a SOSP.

Indeed, the configuration $(0,0,0,0,\pi,\pi,\pi,\pi)$ is not a local minimum of the energy function. When nodes 1,2,3,4 are jointly perturbed slightly away from angle 0 in the same direction, they do not return to the original configuration. Instead, they continue to move toward the π -oriented nodes

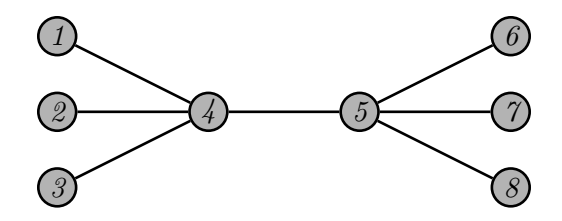


FIGURE 8. At the configuration $(0,0,0,0,\pi,\pi,\pi,\pi)$, each node experiences a force from its neighbors that is aligned with its own direction. However, this configuration is not stable, as can be verified by examining the eigenvalues of the corresponding Hessian matrix.

5, 6, 7, 8, indicating a decrease in energy and confirming that the configuration is unstable. This can be rigorously proven by quadratic form $\mathbf{x}^T \mathbf{H} \mathbf{x}$, we omit it here.

4.4. **Notations.** The below definitions are *nodewise* concept since they are always made with respect to a node in certain state θ . For example, when we say that *node* i attains equilibrium at θ , we mean that

$$\mu_i oldsymbol{v}_i \ = \ \sum_{j \in N(i)} oldsymbol{v}_j, \qquad \mu_i \in \mathbb{R}.$$

Similarly, when we say that node i attains a stable equilibrium at θ , we mean the same balance equation (8) holds with $\mu_i \geq 0$. In the proof of global synchrony for threshold graphs, we frequently use this necessary condition. To make the reasoning more intuitive for the reader, we assign different colors to nodes representing different cases.

	Equation	Illustration
Equilibrium	$egin{aligned} \mu_i oldsymbol{v}_i = \sum_{j \in N(i)} oldsymbol{v}_j, & \mu_i \in \mathbb{R} \end{aligned}$	
Stable equilibrium	$\mu_i \boldsymbol{v}_i = \sum_{j \in N(i)} \boldsymbol{v}_j, \ \mu_i \ge 0$	
Asymptotically stable (positively forced)	$\mu_i \boldsymbol{v}_i = \sum_{j \in N(i)} \boldsymbol{v}_j, \ \mu_i > 0$	· · ·
Zero-forced	$\mu_i \mathbf{v}_i = \sum_{j \in N(i)} \mathbf{v}_j, \ \mu_i = 0$	· ·
Negatively forced		

TABLE 1. Stability classification of node i at equilibrium θ . The sign of μ_i determines the type of stability, visualized by node color.

It is important to note that these definitions do not require the state θ itself to be an equilibrium or stable equilibrium of the system. Indeed, at a given state θ it is possible that some nodes satisfy the condition that their own phasor is parallel to the aggregated phasor formed by their neighbors. Such nodes are in equilibrium at this particular configuration θ ; however, this does not imply that the configuration itself is an equilibrium state, since other nodes may not satisfy the same condition. Nevertheless, if θ is indeed such an equilibrium, then the above conditions are of course implied, according to Lemmas 4.4 and 4.1.

5. Geometric twins and their phasor geometry

In this section, we introduce the concept of $geometric\ twins\ (g-twins\ for\ abbreviation)$, that takes into account the unit vectors $\mathbf{v}_i = (\cos\theta_i, \sin\theta_i)$ associated with each node i in a Kuramoto state $\boldsymbol{\theta}$. Two nodes are said to be g-twins if they satisfy certain geometric relationships at this configuration. It is worth noting that, due to the conceptual similarity, we borrow the term twins from graph theory. However, we precede it with the word geometric to emphasize that our definition depends on the positions of the node phasors in the specific configuration. This concept captures a form of $geometric\ symmetry\$ at $\boldsymbol{\theta}$ that will be crucial in our proof for global synchrony of threshold graphs.

5.1. Closed geometric twins.

Definition 5.1 (Closed g-twins). Let G = (V, E) be a graph and θ a state of the Kuramoto model on G. Two nodes $i, j \in V$ are called *closed g-twins at state* θ if there exists a two-dimensional vector \mathbf{q} such that

$$(\boldsymbol{v}_i \parallel \boldsymbol{v}_j + \boldsymbol{q} \text{ or } \boldsymbol{v}_j + \boldsymbol{q} = \boldsymbol{0})$$
 and $(\boldsymbol{v}_j \parallel \boldsymbol{v}_i + \boldsymbol{q} \text{ or } \boldsymbol{v}_i + \boldsymbol{q} = \boldsymbol{0})$

or equivalently

$$\mathbf{v}_j + \mathbf{q} = \mu_i \mathbf{v}_i$$
 and $\mathbf{v}_i + \mathbf{q} = \mu_j \mathbf{v}_j$ for some $\mu_i, \mu_j \in \mathbb{R}$

where $\mathbf{v}_k = (\cos \theta_k, \sin \theta_k)$ is the unit vector associated with node k.

If moreover both strengths are nonnegative, meaning that each vector \mathbf{v}_i and \mathbf{v}_j points in the same direction as the sum of the other and the common vector \mathbf{q} (or that summation is the zero vector), then we call them *stable closed g-twins*.

Theorem 5.2 (Phasor geometry of closed g-twins). Consider a state θ of the Kuramoto model on graph G = (V, E), the phasor positions of closed g-twins $a, b \in V$ with strength μ_a, μ_b with respect to the common vector falls into one of the following three cases:

- (1) $\mathbf{v}_a = \mathbf{v}_b \text{ and } \mu_a = \mu_b;$
- (2) $\mathbf{v}_a = -\mathbf{v}_b$ and $\mu_a + \mu_b = -2$ and $\mu_a \neq -1$;
- (3) $v_a, v_b \in \mathbb{S}^1$ and $\mu_a = \mu_b = -1$ and $v_a + v_b + q = 0$.

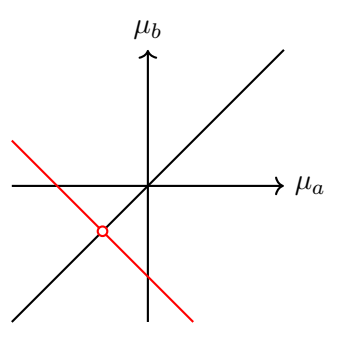


FIGURE 9. Feasible region of strengths (μ_a, μ_b) for closed g-twins. It lies on the lines $\mu_a = \mu_b$ (black, with a and b synchronized) and $\mu_a + \mu_b = -2$ (red, with a and b in antipodal position). At their intersection (-1, -1), marked by a hollow dot, there is no additional constraint on the phasors of a and b.

Proof. According to the definition of closed g-twins

$$\mathbf{v}_b + \mathbf{q} = \mu_a \mathbf{v}_a$$
 and $\mathbf{v}_a + \mathbf{q} = \mu_b \mathbf{v}_b$

we have

$$q = \mu_a \boldsymbol{v}_a - \boldsymbol{v}_b = \mu_b \boldsymbol{v}_b - \boldsymbol{v}_a$$

Thus

$$(\mu_a + 1)\mathbf{v}_a = (\mu_b + 1)\mathbf{v}_b. \tag{13}$$

Case 1: $\mu_a = \mu_b = -1$. In this case, we have

$$q = v_a + v_b$$

Case 2: $\mu_a \neq -1$ and $\mu_b \neq -1$. In this case, from (13), it must hold that

$$v_a \parallel v_b$$

This leads to two subcases: (1) If $\mu_a = \mu_b \neq -1$, then $\mathbf{v}_a = \mathbf{v}_b$; (2) If $\mu_a + 1 = -(\mu_b + 1)$, then equivalently, we have $\mu_a + \mu_b = -2$. This implies $\mathbf{v}_a = -\mathbf{v}_b$.

Definition 5.3 (Stable closed g-twins). Under the setting of Definition 5.1, we say that nodes i and j are stable closed g-twins if furthermore

$$(\boldsymbol{v}_i \Uparrow \boldsymbol{v}_j + \boldsymbol{q} \text{ or } \boldsymbol{v}_j + \boldsymbol{q} = \boldsymbol{0})$$
 and $(\boldsymbol{v}_j \Uparrow \boldsymbol{v}_i + \boldsymbol{q} \text{ or } \boldsymbol{v}_i + \boldsymbol{q} = \boldsymbol{0})$

or equivalently

$$v_j + q = \mu_i v_i$$
 and $v_i + q = \mu_j v_j$ for some $\mu_i, \mu_j \ge 0$.

Similarly, one can define open g-twins and stable open g-twins at state θ , though this concept will not be used in our proofs in this chapter. It may nevertheless be of independent interest in understanding the geometry of non-adjacent nodes with certain geometric symmetries at equilibria.

5.2. Open geometric twins.

Definition 5.4 (Open g-twins). Let G = (V, E) be a graph and θ a state of the Kuramoto model on G. Two nodes $i, j \in V$ are called *open g-twins* at state θ if there exists a two-dimensional vector \boldsymbol{q} such that

$$(\boldsymbol{v}_i \parallel \boldsymbol{q} \text{ and } \boldsymbol{v}_i \parallel \boldsymbol{q}) \text{ or } \boldsymbol{q} = \boldsymbol{0},$$

or equivalently,

$$q = \mu_i v_i = \mu_j v_j$$
 for some $\mu_i, \mu_j \in \mathbb{R}$.

Here $\mathbf{v}_k = (\cos \theta_k, \sin \theta_k)$ is the unit vector associated with node k.

Definition 5.5 (Stable open g-twins). Under the setting of Definition 5.4, we say that nodes i and j form geometric stable open twins if furthermore

$$v_i \uparrow q$$
 or $q = 0$,

and

$$v_i \uparrow q$$
 or $q = 0$,

or equivalently,

$$\mathbf{q} = \mu_i \mathbf{v}_i = \mu_j \mathbf{v}_j$$
 for some $\mu_i, \mu_j \geq 0$.

Remark 5.6. For brevity, whenever the conditions of Definition 5.4 are satisfied, we shall simply say that i and j form open g-twins with strengths (μ_i, μ_j) , with respect to the common vector \mathbf{q} . The terminology for closed g-twins, stable g-twins, and stable closed g-twins is used analogously.

Under the special geometric symmetries described above, the phasors of g-twins exhibit a particular symmetric configuration on the unit circle. This in turn allows us to obtain a precise characterization of the relative positions of the phases θ_i of nodes with such hidden geometric symmetry, both at equilibrium and at stable equilibrium of the Kuramoto model. We refer to the notation on node at (stable) equilibrium in Table 1 for clarity.

Theorem 5.7 (Phasor geometry of open g-twins). Consider a state θ of the Kuramoto model on graph G = (V, E), the phasor positions of open g-twins $a, b \in V$ with strength μ_a, μ_b with respect to the common vector \mathbf{q} falls into one of the following three cases:

- (1) $\mathbf{v}_a = \mathbf{v}_b \text{ and } \mu_a = \mu_b \neq 0;$
- (2) $\mathbf{v}_a = -\mathbf{v}_b \text{ and } \mu_a = -\mu_b \neq 0;$
- (3) $v_a, v_b \in \mathbb{S}^1 \text{ and } \mu_a = \mu_b = 0.$

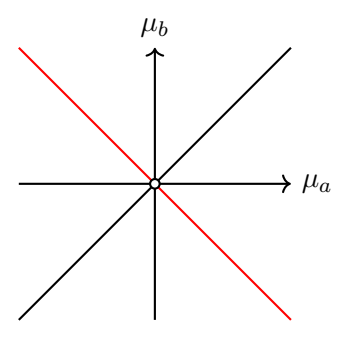


FIGURE 10. Feasible region of strengths (μ_a, μ_b) for open g-twins. It lies on the lines $\mu_a = \mu_b$ (black, corresponding to a and b synchronized) and $\mu_a = -\mu_b$ (red, corresponding to a and b antipodal). At their intersection (0,0), marked by a hollow dot, there is no additional constraint on the phasors of a and b.

Proof. Since

$$\mathbf{q} = \mu_a \mathbf{v}_a = \mu_b \mathbf{v}_b, \tag{14}$$

the following cases arise.

Case 1. $\mu_a = \mu_b = 0$, then we have $\mathbf{q} = 0$.

Case 2. If $\mu_a, \mu_b \neq 0$, then, from 14 we have

$$oldsymbol{v}_a = rac{1}{\mu_a} oldsymbol{q} = rac{\mu_b}{\mu_a} oldsymbol{v}_b.$$

Since $\|\boldsymbol{v}_a\| = \|\boldsymbol{v}_b\| = 1$, it follows that $|\mu_a| = |\mu_b|$. We distinguish two subcases. If $\mu_a = \mu_b$, then $\boldsymbol{v}_a = \boldsymbol{v}_b$. If $\mu_a = -\mu_b$, then $\boldsymbol{v}_a = -\boldsymbol{v}_b$, and one of μ_a, μ_b is negative.

6. Formation of geometric twins

The motivation for introducing g-twins in the previous section comes from the proof of global synchronization on threshold graphs. In that proof, it turns out that synchronization does not rely solely on *structural symmetry* (i.e., forming structural twins), but can also arise from a more general *geometric symmetry*, where the corresponding phasors occupy special symmetric positions on the unit circle.

In this section, we first mention that structural twins at equilibrium constitute the simplest case of forming g-twins. We then move on to more general situations where nodes are not structural twins, yet under both specific geometric conditions (on the phasors) and accompanying structural

conditions, they still form g-twins. Both cases will play a crucial role in the proof of global synchronization for threshold graphs.

6.1. Structural twins at equilibrium.

Definition 6.1 (Structural Twins). Let G = (V, E) be a graph. Two nodes $i, j \in V$ are called structural closed twins if

$$N[i] = N[j], \tag{15}$$

and structural open twins if

$$N(i) = N(j), \tag{16}$$



Figure 11. Illustration of structural twins.

Remark 6.2. In the discussion above we used the term structural to emphasize that whether two nodes are twins depends purely on the graph structure. In graph theory they are simply called true or adjacent twins, and false or non-adjacent twins.

Clearly, if θ is an equilibrium point of the Kuramoto model with respect to graph G, and two nodes a and b satisfy condition 15, then they must form a pair of closed g-twins. This is because, according to Lemma 4.1, the nodes a and b are structurally symmetric (satisfying (15)) 8, that is

$$\begin{cases} \sum_{j \in N(a)} \mathbf{v}_i = \mu_a \mathbf{v}_a, & \mu_a \in \mathbb{R} \\ \sum_{j \in N(b)} \mathbf{v}_j = \mu_b \mathbf{v}_b, & \mu_b \in \mathbb{R} \end{cases}$$

$$oldsymbol{q} = \sum_{j \in N(a) \setminus \{b\}} oldsymbol{v}_j = \sum_{j \in N(b) \setminus \{a\}} oldsymbol{v}_j$$

such that $v_b + q = \mu_a v_a$ and $v_a + q = \mu_b v_b$ for some $\mu_a, \mu_b \in \mathbb{R}$, according to notations in 4.4. The relative positions of nodes a and b on the unit circle, together with their nodewise stability in this case, are illustrated in Figure 14.

There, colors indicate node-wise stability: Blue indicates $\mu > 0$ (stable), red for $\mu < 0$ (unstable), black for $\mu = 0$.

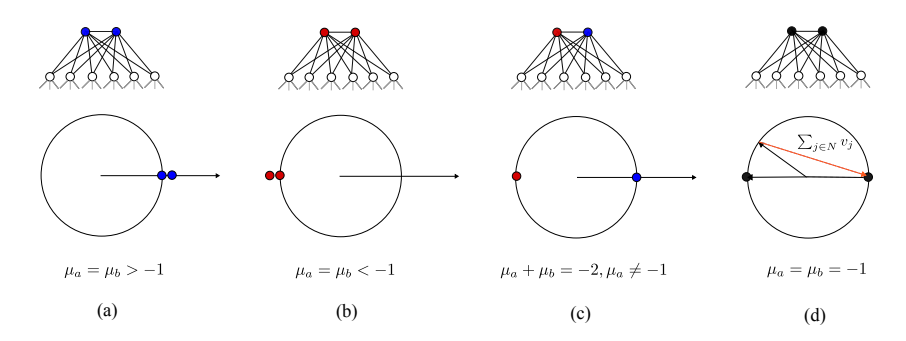


FIGURE 12. Structural closed twins attaining nodewise equilibrium.

Remark 6.3. Here the case (d) is detailed in the following figure. One can clearly see that

$$\boldsymbol{v}_a + \boldsymbol{v}_b + \boldsymbol{q} = \boldsymbol{0},$$

where N denotes the set of common neighbors of a and b, excluding each other.

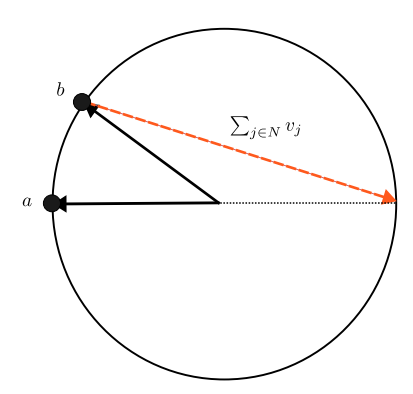


FIGURE 13. Geometric illustration of case (d) for false twins at equilibrium. The red arrow represents the vector sum \mathbf{q} , where N is the common neighborhood of nodes a and b, excluding each other. In this case, $\mu_a = \mu_b = -1$, and the three vectors \mathbf{v}_a , \mathbf{v}_b , and \mathbf{q} form a triangle summing to zero.

Similarly, structural open twins a, b at equilibrium in θ are also geometric open twins, since there exists

$$oldsymbol{q} = \sum_{j \in N(a)} oldsymbol{v}_j = \sum_{j \in N(b)} oldsymbol{v}_j$$

such that $\mathbf{q} = \mu_a \mathbf{v}_a$ and $\mathbf{q} = \mu_b \mathbf{v}_b$ for some $\mu_a, \mu_b \in \mathbb{R}$, according to notations in 4.4. The relative positions of nodes a and b on the unit circle, together with their nodewise stability in this case, are illustrated in Figure 14. The same as in the above mentioned closed twins case, that colors indicate their stability.

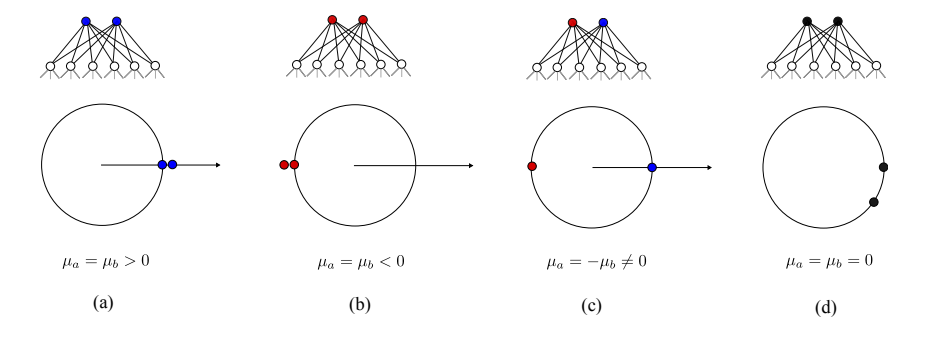
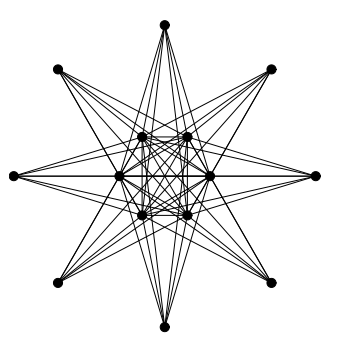


FIGURE 14. Structural open twins attaining nodewise equilibrium.

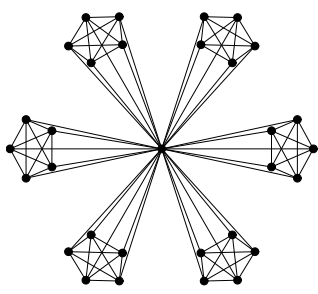
Our strategy for proving that a given graph admits global synchronization is to characterize the positions of all nodes at stable equilibrium (in fact, more general, at SOSP of $E(\theta)$). Furthermore, the lemma on structural twins at equilibrium shows that whenever two structural twins both attain stable equilibrium, they must synchronize if they are closed twins. It is worth noting, however, that in the case of open twins, synchronization is not guaranteed: it may happen that both strengths μ_i and μ_j vanish, in which case the phasors of i and j remain unconstrained.

At this point, we are already able to characterize certain new classes of globally synchronizing graphs, according to results in this section.

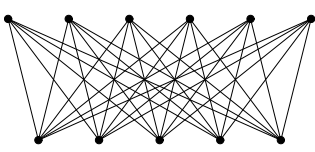
Theorem 6.4. Complete split graphs, windmill graphs, complete bipartite graphs are globally synchronizing.



(A) Complete split graphs.



(B) Windmill graphs $W_{5,6}$.



(c) Complete bipartite.

6.2. Synchronous pendant extension. In this section, we present a scenario in which a group of nodes forms closed g-twins without being structural closed twins, that is called *synchronous* pendant extension. Specifically, consider a set S that satisfies the structural assumption that the additional neighborhood of some subset $S_1 \subseteq S$ is attached to S_1 in a leaf-like manner. The geometric assumption, on the other hand, is that this additional neighborhood synchronizes with S_1 .

To prepare for the presentation and proof of Lemma 6.6, we first establish Lemma 6.5, which highlights the following fact: If there exists a synchronized, fully connected set S of nodes with a synchronized pendant attached, then each node in S is aligned with the vector sum of the phasors of its remaining neighbors, namely those not in S nor in the pendant. From the perspective of synchronization propagation, this can be interpreted as synchronization spreading from S together with its pendant to the group of all other neighbors.

Lemma 6.5. Let G = (V, E) be a graph, and suppose there exists a subset of nodes $W \subseteq V$ partitioned into four disjoint subsets:

$$W = Q \cup S \cup P$$
.

under the following structural assumptions:

- (i) For all $i \in Q$, we have $N(i) \subseteq S$;
- (ii) The subgraph G[S] is a complete graph;
- (iii)For any $i \in S$, its neighbourhood consists of the set P, its neighbours in Q, and the rest of the clique $S \setminus \{i\}$.

Assume further that all nodes in $Q \cup S$ are synchronized, i.e., there exists \mathbf{v} such that $\mathbf{v}_i = \mathbf{v}_j = \mathbf{v}$, $\forall i, j \in Q \cup S$. Then

$$\sum_{i \in P} v_i \uparrow v \quad or \quad \sum_{i \in P} v_i = 0.$$

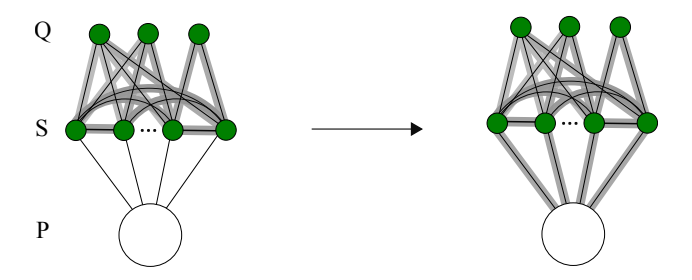


FIGURE 16. Illustration of Lemma 6.5. Elements in the figure follow the same conventions as in Figure 18. Moreover, a large node represents a set of nodes. An edge from a small node A_i to a large node S indicates that A_i is connected to all nodes in S. The diagram depicts a configuration where a set of synchronized "false twin-like" nodes, with differing but synchronized neighbors, implies that their shared neighbors (the large white node) sum to a vector pointing in the same direction as the synchronized nodes.

Proof. For any node $i \in S$,

$$N(i) = Q \cup (S \setminus \{i\}) \cup P \tag{17}$$

and

$$\sum_{j \in N(i)} \mathbf{v}_j = \mu_i \mathbf{v}_i. \tag{18}$$

Plug (17) into (18), we obtain

$$\sum_{j \in Q \cup (S \setminus \{i\}) \cup P} \boldsymbol{v}_j = \mu_i \boldsymbol{v}_i.$$

Since $Q \cup S$ synchronize, we have

$$(|Q| + |S| - 1)\boldsymbol{v}_i + \sum_{j \in P} \boldsymbol{v}_j = \mu_i \boldsymbol{v}_i, \text{ where } \mu_i \ge 0.$$

Thus

$$\sum_{i \in P} \boldsymbol{v}_j = (\mu_i - (|Q| + |S| - 1)) \, \boldsymbol{v}_i, \quad \text{where} \quad \mu_i \ge 0.$$

Now, we are left to show $\mu_i - (|Q| + |S| - 1) < 0$ is not possible. Indeed, let v be an n-dimensional vector where the i-th element is one if $i \in Q \cup S$, and zero otherwise. Then

$$\mathbf{v}^{T}H\mathbf{v} = \sum_{i \in Q \cup S} \sum_{j \in P} \cos(\theta_{i} - \theta_{j})$$

$$= \sum_{i \in S} \sum_{j \in P} \cos(\theta_{i} - \theta_{j})$$

$$= \sum_{i \in S} \sum_{j \in P} \mathbf{v}_{i} \cdot \mathbf{v}_{j}$$

$$= \sum_{i \in S} \mathbf{v}_{i} \cdot \sum_{j \in P} \mathbf{v}_{j}$$

$$= |S|\mathbf{v}_{i} \cdot \sum_{j \in P} \mathbf{v}_{j}$$

$$= |S|\mathbf{v}_{i} \cdot \sum_{j \in P} \mathbf{v}_{j}$$
(19)

where the second equality is due to there is no connection between Q and P. Clearly, if $\mu_i - (|Q| + |S| - 1) < 0$, then the above form is negative, and this contradicts to the stability of θ . The proof is complete.

We are now ready to present the case of a *synchronous pendant*, which constitutes one possible configuration leading to the formation of *geometric stable closed twins*. This case will serve as one of the core lemmas in our proof for threshold graphs.

Consider a set of nodes S attaining stable equilibrium at θ which induces a clique⁴. S can be divided into S_1 which connects only to a set P, and a synchronized group S_2 which in addition connects to a synchronized pendant set⁵ Q. We will show that although S_1 and S_2 are not structurally identical, this difference, arising from the synchronous pendant, does not interfere with synchronization, in other words, the two groups behave as geometric stable closed twins.

The proof of Lemma 6.6 is based on Lemma 6.5. If we can decompose the set P there into $\{A\} \cup P$, where A connects to all nodes in S, and all nodes in P, then we have the following Lemma.

Lemma 6.6. Let G = (V, E) be a graph, and suppose there exists a subset of nodes $W \subseteq V$ partitioned into four disjoint subsets:

$$W = Q \cup S_1 \cup S_2 \cup P.$$

under the following structural assumptions:

- (i) For all $i \in Q$, we have $N(i) \subseteq S_1$;
- (ii) The subgraph $G[S_1 \cup S_2]$ is a complete graph;
- (iii) For any $i \in S_1 \cup S_2$, its neighbourhood can be decomposed into three parts: the set P, its neighbours inside Q, and the rest of the clique $S_1 \cup S_2$. Formally, if we denote $Q_i = N(i) \cap Q$, then

$$N(i) = P \cup Q_i \cup ((S_1 \cup S_2) \setminus \{i\}).$$

Equivalently,

$$N(i) \setminus (Q \cup (S_1 \cup S_2)) = P.$$

Assume further that all nodes in $Q \cup S_1$ are synchronized, i.e.,

$$v_i = v_j, \quad \forall i, j \in Q \cup S_1.$$

Then the set $S_1 \cup S_2$ forms a group of geometric stable closed twins, therefore they synchronize.

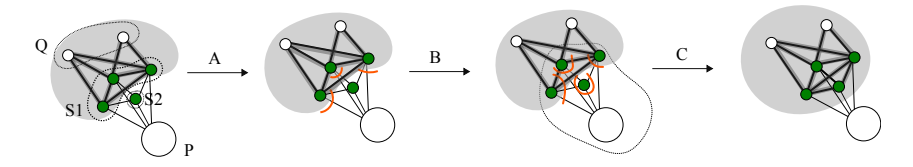


FIGURE 17. Illustration of Lemma 6.6. Elements follow the same conventions as in previous figures. The gray-shaded nodes are synchronized; an edge with a gray background indicates synchronization between the corresponding nodes. Each orange arc separates a small blue node from a group of nodes it connects to, indicating that the vector of the blue node is in the same direction as the sum of the vectors of the nodes on the opposite side of the arc. The figure illustrates how the synchronized block $A \cup S_1$ extends to include S_2 through propagation enabled by the specific local structure.

⁴Forming a clique guarantees the "closed" property required for closed twins.

 $^{^5}$ Specifically, Q can be understood as a generalization of a leaf attached to one node, and it is well known that the presence of a leaf does not affect the stability of the state.

Proof. Observe that the set S_1 induces a fully-connected subgraph, and Q is a synchronous pendant to S_1 , then according to Lemma 6.6, we have

$$\forall i \in S_1, \quad \boldsymbol{v}_i \uparrow \sum_{k \in S_2 \cup P} \boldsymbol{v}_k \quad \text{or} \quad \sum_{k \in S_2 \cup P} \boldsymbol{v}_k = \boldsymbol{0}.$$

Combine this with the fact

$$v_i = v_j \quad \forall i \in S_1, j \in S_2,$$

we obtain

$$\forall i \in S_1, \quad \boldsymbol{v}_i \Uparrow \sum_{k \in S_2 \cup P} \boldsymbol{v}_j + \sum_{k \in S_1 \setminus \{i\}} \boldsymbol{v}_j \quad \text{or} \quad \sum_{k \in S_2 \cup P} \boldsymbol{v}_k + \sum_{k \in S_1 \setminus \{i\}} \boldsymbol{v}_k = \boldsymbol{0}.$$

Equivalently, we can write

$$\forall i \in S_1, \quad \mathbf{v}_i \uparrow \sum_{k \in S_1 \cup P \cup S_2 \setminus \{i\}} \mathbf{v}_k \quad \text{or} \quad \sum_{k \in S_1 \cup P \cup S_2 \setminus \{i\}} \mathbf{v}_k = \mathbf{0}.$$
(20)

Another observation is on nodes in S_2 that

$$\forall i \in S_2, \quad \boldsymbol{v}_i \Uparrow \sum_{k \in S_2 \setminus \{i\}} \boldsymbol{v}_k + \sum_{j \in S_1 \cup P} \boldsymbol{v}_k \quad \text{or} \quad \sum_{k \in S_2 \setminus \{i\}} \boldsymbol{v}_k + \sum_{j \in S_1 \cup P} \boldsymbol{v}_k = \boldsymbol{0}$$

since every node in S_2 attains stable equilibrium in θ . Equivalently, we can write

$$\forall i \in S_2, \quad \mathbf{v}_i \uparrow \sum_{k \in S_1 \cup P \cup S_2 \setminus \{i\}} \mathbf{v}_k \quad \text{or} \quad \sum_{k \in S_1 \cup P \cup S_2 \setminus \{i\}} \mathbf{v}_k = \mathbf{0}.$$
(21)

Combined the facts 20 and 21, we get nodes in $S_1 \cup S_2$ are geometric stable closed twins.

7. Main proof: the induction argument

7.1. **One more key lemma.** To complete the argument, we establish one more lemma prior to the proof of the main theorem.

Lemma 7.1 (Synchronization of closed twins with common neighbour). Let $S \subseteq V$ be a set of structural closed twins in a graph G, and let among their common neighbourhood, there exists a node A such that its neighbourhood is exactly S, i.e., N(A) = S. Assume that all nodes in $S \cup \{A\}$ attain stable equilibrium at configuration θ , that is,

$$\forall i \in S \cup \{A\}, \quad \mu_i v_i = \sum_{j \in N(i)} v_j \quad \text{with} \quad \mu_i \ge 0,$$

then the nodes in $S \cup \{A\}$ synchronize at θ .

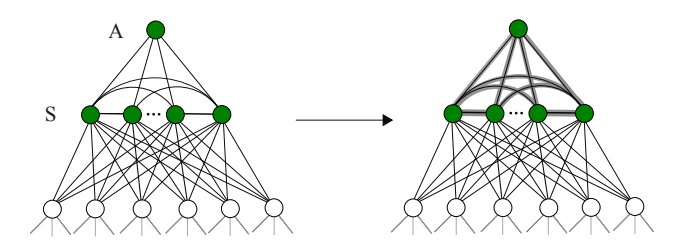


FIGURE 18. Illustration of Lemma 7.1. All green nodes attain stable equilibrium. The set S (middle row) forms a set of false twins, and node A (top) has neighborhood exactly S. Thin lines represent the edges in the original graph. The conclusion is that all green nodes must synchronize, indicated by the thick edges in the right diagram.

Proof. Since S forms a set of structural stable closed twins, we have $i, j \in S$, we have $v_i = v_j$ and let us denote this common phasor as v. Moreover, since A only connects to the set S which is synchronizing, and it attains stable equilibrium at θ , we have

$$\mu_A \boldsymbol{v}_A = \sum_{j \in N(A)} \boldsymbol{v}_j = \sum_{j \in S} \boldsymbol{v}_j = |S| \boldsymbol{v}$$

Thus $\mathbf{v}_A = \mathbf{v}$. The proof is complete.

7.2. Illustrative example. In this section, we present a simple but general enough example to illustrate how to use Lemma 6.6 and 7.1 to establish global synchronization of connected threshold graphs. Specifically, to show how synchronization starts from a local substructure and eventually propagates to the entire threshold graph. The proof for all connected threshold graphs follows the same idea, with additional work needed for full generalization.

Let us take a look at the threshold graph corresponding to the sequence

01010101

We use capital letters to represent the nodes corresponding to each bit in the sequence, including the initial starting node.

The corresponding threshold graph is shown as follows.

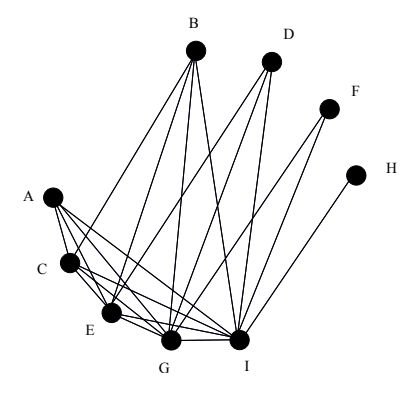


FIGURE 19. Threshold graph corresponding to the sequence 01010101, with vertices labeled A to I in the order of their addition.

Concluding global synchronization step by step. To show that this graph globally synchronizes, we prove that any second order stationary point $\boldsymbol{\theta}$ of $E_G(\boldsymbol{\theta})$ on the threshold graph must be synchronous. Clearly, any second order stationary point $\boldsymbol{\theta}$ is also a local minimum of $E_G(\boldsymbol{\theta})$ or stable equilibrium of the Kuramoto model 2. Thus, the Lemmas established in Chapter 4 applies here. That is, every node attains stable equilibrium in $\boldsymbol{\theta}$, according to Lemma 4.4.

We will use Lemmas 6.6 and 7.1 repeatedly in the following illustration.

Step 1. Start with the edge between H and I. Synchronization between nodes H and I can be obtained from stability condition of H soely. Indeed, since H attains stable equilibrium at $\boldsymbol{\theta}$, there exists $\mu_H \geq 0$ such that $\mu_H \boldsymbol{v}_H = \sum_{j \in N(H)} \boldsymbol{v}_j$ and we know that $\sum_{j \in N(H)} \boldsymbol{v}_j = \boldsymbol{v}_I$, we obtain $\boldsymbol{v}_H = \boldsymbol{v}_I$. One could also use Lemma to argue $\boldsymbol{v}_H = \boldsymbol{v}_I$, as this is the simplest case of the lemma.

Step 2. Observe that the pair of node G and I forms geometric stable closed twins at $\boldsymbol{\theta}$. Indeed, the only difference between N[G] and N[I] is that I additionally has a synchronizing pendant H. Thus $\boldsymbol{v}_G = \boldsymbol{v}_I$. Now nodes G, I, H are synchronized.

Step 3. Note that node F connects to G and I which are synchronized as established in Step 2, we have $\mathbf{v}_F = \mathbf{v}_G = \mathbf{v}_I$, according to Lemma.

Step 4. Observe that nodes E, G, I induce a fully connected subgraph, and nodes G and I have additional synchronizing pendant, therefore, according to Lemma 6.6, three of them form geometric stable closed twins. Thus, $\mathbf{v}_E = \mathbf{v}_G = \mathbf{v}_I$.

Step 4. Observe that node D connects to E, G, I which are synchronzed, thus $\mathbf{v}_D = \mathbf{v}_E = \mathbf{v}_G = \mathbf{v}_I$, according to Lemma.

Step 5. Observe that nodes C, E, G, I induce a fully-connected subgraph, and among them, nodes E, G, I admit additional synchronizing pendant D, F, H. Consequently C, E, G, I form a group of geometric stable closed twins, and therefore they synchronize.

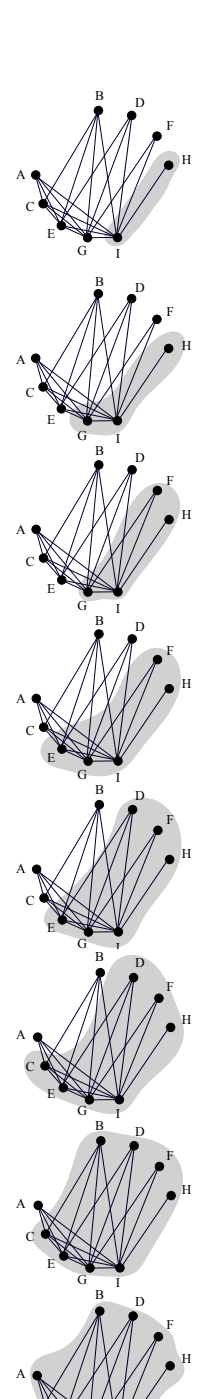
Step 6. Now note that the node B connects to a group of synchronzing nodes C, E, G, I. Therefore according to Lemma, node B synchronzes with them as well. That is, $\mathbf{v}_B = \mathbf{v}_C = \mathbf{v}_E = \mathbf{v}_G = \mathbf{v}_I$.

Step 7. Observe that nodes A, C, E, G, I induce a fully-connected subgraph, and among them, nodes C, E, G, I admit additional synchronzing pendant B, D, F, H. Consequently A, C, E, G, I form a group of geometric stable closed twins, and therefore they synchronize.

In conclusion, θ is a synchronized state, and thus the threshold graph globally synchronizes.

7.3. **Main proof.** Before proceeding, we introduce some notation. Any connected threshold graph can be specified by a bit sequence consisting of alternating blocks of 1's and 0's. Since the graph is connected, the last bit must be 1. We group the sequence into maximal contiguous blocks of 1's and 0's. Let U_1, U_2, \ldots, U_k denote the blocks of 1's (indexed from bottom to top), and let I_i denote the 0-block directly above U_i (if any). Thus, the sequence takes the form either

$$U_1, I_2, U_2, \dots, I_{k-1}, U_{k-1}, I_k, U_k,$$



depending on whether the sequence begins with a 0-block.

Proof of Theorem 1.2. We prove the main theorem 1.2 by induction. First, assume θ is a second-order stationary point of $E(\theta)$. Our goal is to show $\theta_1 = \cdots = \theta_n$. Let the sequence defining the threshold graph consist of maximal contiguous blocks of 1's and 0's, arranged as either:

$$U_1, I_1, U_2, I_2, \dots, U_k$$
 or $I_0, U_1, I_1, U_2, I_2, \dots, U_k$.

Base case. At a stable equilibrium θ , the last block U_k must synchronize. This follows directly from Lemma 5.2, as the nodes in U_k are false twins and thus must synchronize.

Inductive hypothesis. Assume that the nodes in the last m blocks of 1's, U_{k-m+1}, \ldots, U_k , are synchronized.

Inductive step. Here, we show that the synchronization of $\bigcup_{i=k-m+1}^k U_i$ propagates to $\bigcup_{i=k-m}^k U_i$, since the preceding block U_{k-m} must synchronize with $\bigcup_{i=k-m+1}^k U_i$. Indeed, since all nodes in $\bigcup_{i=k-m+1}^k U_i$ synchronize, any node added as isolated nodes whose neighbourhood is a subset of $\bigcup_{i=k-m+1}^k U_i$ must synchronize with them as well. These nodes are exactly nodes in $\bigcup_{i=k-m+1}^k I_i$. That is, every nodes $i, j \in \bigcup_{i=k-m+1}^k U_i \cup I_i$ satisfy $v_i = v_j$.

Observe that $\bigcup_{i=k-m+1}^{k} I_i$ are in fact synchronizing pendant attaches to $\bigcup_{i=k-m+1}^{k} U_i$, and they are the only difference of neighbourhood between the U_{k-m} and $\bigcup_{i=k-m+1}^{k} U_i$, thus according to Lemma 6.6, nodes in $\bigcup_{i=k-m}^{k} U_i$ form a set of geometric stable closed twins, and they must synchronize.

Conclusion. All nodes in $\bigcup_{i=1}^k (U_i \cup I_i)$ or $I_0 \cup \left(\bigcup_{i=1}^k (U_i \cup I_i)\right)$ synchronize. Namely $\theta_1 = \cdots = \theta_n$, thus any threshold graph is globally synchronizing as long as it is connected.

Acknowledgements. We would like to thank Afonso S. Bandeira for an insightful discussion at the early stage of this work.

References

- [ABV⁺05] Juan A. Acebrón, Luis L. Bonilla, Conrad J. Pérez Vicente, Felix Ritort, and Renato Spigler. The kuramoto model: A simple paradigm for synchronization phenomena. *Reviews of Modern Physics*, 77(1):137–185, 2005.
- [AK06] P.-A. Absil and K. Kurdyka. On the stable equilibrium points of gradient systems. Systems & Control Letters, 55(7):573–577, 2006.
- [BB68] John Buck and Elisabeth Buck. Mechanism of rhythmic synchronous flashing of fireflies. *Science*, 159(3821):1319–1327, 1968.
- [Bha07] Rajendra Bhatia. Positive Definite Matrices. Princeton University Press, Princeton, NJ, 2007.
- [BHSW13] Daniel J. Bates, Jonathan D. Hauenstein, Andrew J. Sommese, and Charles W. Wampler. Bertini: Software for Numerical Algebraic Geometry. Available at bertini.nd.edu, 2013.
- [CRMB24] Christopher Criscitiello, Quentin Rebjock, Andrew D. McRae, and Nicolas Boumal. Synchronization on circles and spheres with nonlinear interactions. arXiv preprint arXiv:2405.18273, 2024.
- [DB13] Florian Dorfler and Francesco Bullo. Synchronization and transient stability in power networks and non-uniform kuramoto oscillators. SIAM Journal on Control and Optimization, 50(3):1616–1642, 2013.
- [DB14] Florian Dörfler and Francesco Bullo. Synchronization in complex networks of phase oscillators: A survey. *Automatica*, 50(6):1539–1564, 2014.
- [GLPR23a] Borjan Geshkovski, Cyril Letrouit, Yury Polyanskiy, and Philippe Rigollet. A mathematical perspective on transformers. arXiv preprint arXiv:2312.10794, 2023.
- [GLPR23b] Borjan Geshkovski, Cyril Letrouit, Yury Polyanskiy, and Philippe Rigollet. A mathematical perspective on transformers. arXiv preprint arXiv:2312.10794, 2023.
- [HJ85] Roger A. Horn and Charles R. Johnson. *Matrix Analysis*. Cambridge University Press, Cambridge, UK, 1st edition, 1985.
- [Kha02] Hassan K. Khalil. Nonlinear Systems. Prentice Hall, Upper Saddle River, NJ, 3rd edition, 2002.

- [Kur75] Yoshiki Kuramoto. Self-entrainment of a population of coupled non-linear oscillators. In *International Symposium on Mathematical Problems in Theoretical Physics*, pages 420–422. Springer, 1975.
- [MP95] N. V. R. Mahadev and U. N. Peled. Threshold Graphs and Related Topics, volume 56 of Annals of Discrete Mathematics. Elsevier Science Publishers, 1995.
- [MS06] Alexander S. Mikhailov and Kenneth Showalter. Control of waves, patterns and turbulence in chemical and biological systems. *Physics Reports*, 425(2-3):79–194, 2006.
- [PS95] Rossella Petreschi and Andrea Sterbini. Synchronization and threshold graphs. *Theoretical Computer Science*, 143(1):169–183, 1995.
- [SS93] Steven H. Strogatz and Ian Stewart. Coupled oscillators and biological synchronization. *Scientific American*, 269(6):102–109, 1993.
- [Str00] Steven H. Strogatz. From kuramoto to crawford: exploring the onset of synchronization in populations of coupled oscillators. *Physica D*, 143(1-4):1-20, 2000.
- [Win67] Arthur T. Winfree. Biological rhythms and the behavior of populations of coupled oscillators. *Journal of Theoretical Biology*, 16(1):15–42, 1967.

$$\label{eq:complex} \begin{split} & ETH \ Z\"{u}rich, \ Z\"{u}rich, \ Switzerland} \\ & \textit{Email address: } \ \texttt{hongjin-wu@outlook.com} \end{split}$$

ETH ZÜRICH, ZÜRICH, SWITZERLAND *Email address*: ubrandes@ethz.ch